Journal of Magnetic Resonance **144,** 45–52 (2000)
doi:10.1006/jmre.2000.2017, available online at http://www.idealibrary.com on IDEAL®

Two-Pulse Nutation Echoes Generated by Gradients of the Radiofrequency Amplitude and of the Main Magnetic Field

Ioan Ardelean,[1] Attila Scharfenecker, and Rainer Kimmich

Sektion Kernresonanzspektroskopie, Universität Ulm, 89069 Ulm, Germany

Received August 4, 1999; revised December 29, 1999

A two-pulse NMR nutation spectroscopy scheme is suggested that leads to a new type of spin echoes. The amplitude of the radiofrequency (RF) pulses as well as the external magnetic field are assumed to be subject to gradients G_1 and G_0, respectively, in the same but otherwise arbitrary direction. Multiple echoes are predicted and observed at times $k(G_1/G_0)\tau_1$ and $\tau \mp k(G_1/G_0)\tau_1$ ($k = 1, 2, 3, \ldots$) after the second RF pulse, where τ_1 represents the radiofrequency pulse duration, and τ is the spacing of the RF pulses. Based on these echoes, a method for diffusion measurements is proposed that simultaneously provides the spin–lattice relaxation time and the self-diffusion coefficient. © 2000 Academic Press

Key Words: **nutation; radiofrequency amplitude gradients; demagnetizing field; multiple echoes; rotary echoes.**

1. INTRODUCTION

Since the discovery of rotary echoes by Solomon (*1*), the use of gradients of the radiofrequency (RF) amplitude has proved to be of interest for self-diffusion and flow measurements (*2–5*) as well as for NMR imaging (*6, 7*). A review of the possibilities and applicability of this technique can be found in Ref. (*8*).

The methods for self-diffusion or flow measurements suggested so far consist of two pulses of the RF amplitude gradient with an evolution interval τ in between. The gradients of the RF amplitude are assumed to be aligned along the x axis of the laboratory frame, so that spatially varying flip angles $\alpha(x)$ are produced. The first pulse splits the equilibrium magnetization in longitudinal and transverse components both modulated along the x axis. Neglecting relaxation and diffusion processes during the pulses and assuming that the transverse magnetization component is completely spoiled during τ, the longitudinal component is the only one that can provide information about diffusion or spin–lattice relaxation.

The second pulse splits the longitudinal magnetization remaining at the end of the evolution interval again into transverse and longitudinal components. The transverse component is modulated along the x axis of the laboratory frame. No signal arises on these grounds because the average transverse magnetization in the sample is zero. These coherences were therefore considered irrelevant in this context (*8*). The longitudinal component was merely suggested to be read out with the aid of a "homogeneous" 90° pulse. This 90° pulse can be generated either electronically (*8*) by using a second RF coil producing homogeneous RF fields or with the aid of an "adiabatic" RF pulse (*9*). The signal recorded in this way was shown to be subject to diffusion and spin–lattice relaxation in the τ interval.

The first objective of this work is to propose a much simpler method providing the same information: Both RF pulses are subject to the same amplitude gradient. No homogeneous 90° pulse is needed. The longitudinal magnetization component after the second RF pulse then influences the evolution of the transverse component only due to demagnetizing field effects.

In the method to be described, a constant gradient G_0 of the main magnetic field B_0 is additionally employed in the same direction as the gradient G_1 of the RF field amplitude B_1. As a consequence, the coherences underlying the transverse component are refocused and form spin echoes (*10–13*). Note that the gradient G_0 need not be pulsed. On the contrary, keeping it stationary helps to dephase undesired coherences after the first RF pulse. Actually, gradients of the external magnetic field due to intentionally imperfect shimming may be sufficient for this purpose.

As concerns RF, only a single coil is needed for transmitting as well as receiving purposes. In order to have a strong and reasonably constant gradient of the RF amplitude, we have used a conic coil shape (see Fig. 1) as described under Experimental. Other coil geometries (*5, 8, 14*) may be suitable as well.

Another objective of this work is to demonstrate theoretically and experimentally that *multiple nonlinear echoes* are generated by a two-pulse RF gradient sequence in high enough magnetic fields. The origin of these echoes is coherence evolution in the modulated demagnetizing field produced by the longitudinal magnetization component after the second RF pulse. This experiment will be called "two-pulse nutation experiment" leading to "two-pulse nutation echoes" in contrast to the single-pulse nutation variant treated in Ref. (*13*). Both cases represent mixed rotating-frame/laboratory frame coherence evolution schemes, that is, coherences partly evolve under rotating-frame conditions and partly in the form of free evo-

[1] On leave from the Department of Physics, Technical University, 3400 Cluj-Napoca, Romania.

1090-7807/00 $35.00

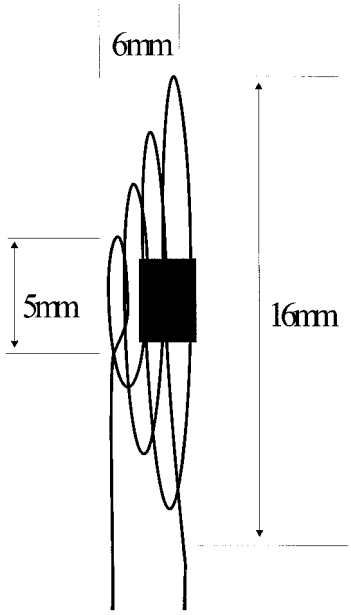

FIG. 1. Geometry of the conic coil used for the production of gradients of the RF amplitude. This coil was used both as transmitter and as receiver coil. The B_1 gradient underlying the RF pulses and the gradient G_0 of the main magnetic field are assumed along the x axis of the laboratory frame.

lution. A pure rotating-frame experiment leading to multiple-rotary echoes as counterparts to the conventional rotary echo (*1*) was described in Ref. (*13*).

2. THEORY

Let us consider an ensemble of uncoupled spins $I = \frac{1}{2}$ subject to the pulse sequence shown in Fig. 2. The term "uncoupled" is to be understood in the sense that there is no indirect (or J) coupling and that short-distance intermolecular dipolar coupling is averaged to zero by molecular motion. The criterion for the latter is determined by the root-mean-squared displacement the spin-bearing particles reach in the course of the evolution time. In liquids of low viscosity, this "motional averaging zone" has a diameter in the order of micrometers. That is, the only couplings to be taken into account here refer to a length scale far beyond any molecular dimension. Long-distance dipolar coupling involves many particles by nature. It is usually taken into account in the continuum (or mean-field) limit that can be treated with the aid of the *demagnetizing field* at the sites of the dipoles to be considered (*15–20*).

The demagnetizing field depends on the spatial distribution of the magnetization. $\mathbf{M}(\mathbf{r})$ and, as a consequence, also on the shape of the sample (*16*). If the magnetization is distributed homogeneously in all ellipsoidal sample, the demagnetizing field is homogeneous as well and even exactly cancels at the position of the probe nuclei if the sample shape is spherical. Provided that the RF gradient is strong enough, any sample shape effects can be neglected and we restrict ourselves to the case in which the magnetization becomes spatially dependent owing to the evolution during the pulse. This in particular means that a modulation of the magnetization along a direction with unit vector $\mathbf{u}_s$ arises. The spatial distribution of the resulting demagnetizing field is then given by (*15*)

$$\mathbf{B}_d(\mathbf{r}) = \mu_0 \Delta \left[M_z(s)\mathbf{u}_z - \frac{1}{3}\mathbf{M}(s) \right], \qquad [1]$$

where

$$\Delta = \frac{3(\mathbf{u}_s \cdot \mathbf{u}_z)^2 - 1}{2} \qquad [2]$$

and μ_0 is the magnetic field constant. Here the coordinate along the $\mathbf{u}_s$ direction is $s = \mathbf{r} \cdot \mathbf{u}_s$ and the unit vector $\mathbf{u}_z$ is directed along the magnetic field relevant for coherence evolution. In the absence of RF irradiation, this field is given by the external magnetic flux density $\mathbf{B}_0 = B_0\mathbf{u}_z$. If the RF gradient is not strong enough the sample shape effects have to be considered numerically (*23*).

As a consequence, any spatial modulation of the magnetization leads to small but finite demagnetizing fields superimposed to the external magnetic field. As concerns the z component, such a modulation is already produced by the RF excitation pulses which are assumed to be subject to a sufficiently strong B_1 gradient. The length scale on which the point symmetry of the magnetization distribution is broken by this inhomogeneous excitation depends on the strength of the B_1 gradient and the pulse width τ_1. Under realistic circumstances it is again extremely long relative to molecular dimensions and typically exceeds 10 μm, that is, the continuum limit is very safely fulfilled.

For the treatment of the two-pulse nutation experiment represented by the pulse sequence in Fig. 2, we assume that the RF field amplitude is always and everywhere in the sample much larger than the demagnetizing field that arises as a consequence of the z magnetization grid set up in the course of the B_1 gradient pulses. Otherwise the field effective in the rotating

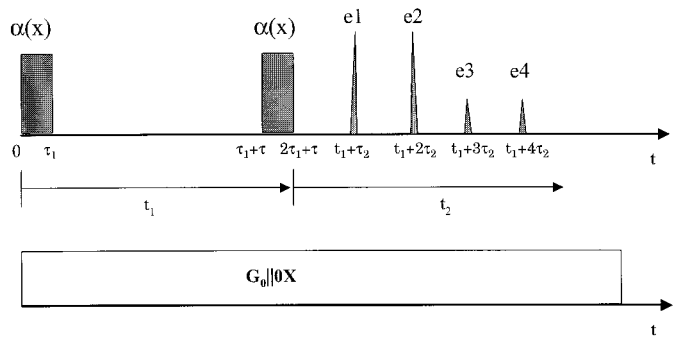

FIG. 2. Sequence for the generation of two-pulse nutation echoes. The phase of the RF pulses is arbitrary. The only condition is that the direction of the external gradient $\mathbf{G}_0$ and of the RF gradients $\mathbf{G}_1$ coincide.

frame would locally deviate somewhat from $\mathbf{B}_1$ due to off-resonance contributions.

The RF pulse amplitude B_1 is subject to a strong gradient across the sample. The flip angle then becomes a function of the position along the B_1 gradient direction, i.e., $\alpha = \alpha(\mathbf{r})$. If the gradient is strong enough, the RF pulse flips the local magnetization vectors in such a way that they are distributed in different directions along the B_1 gradient axis. In case the B_1 gradient is spatially constant within the sample, which, for simplicity, will be assumed in the following, the longitudinal as well as the transverse magnetization components will be modulated periodically along the B_1 gradient direction.

In the pulse scheme shown in Fig. 2 the rotating-frame phase direction is arbitrarily chosen to be x. The B_0 and B_1 gradients are both assumed along the x axis of the laboratory frame. Based on the linear Taylor expansion term of the equilibrium density operator, the spin states generated by the first excitation pulse can be represented by the reduced density operator deprived from all constant terms and factors as

$$\sigma(x, \tau_1) = I_y \sin[\alpha(x, \tau_1)] + I_z \cos[\alpha(x, \tau_1)], \qquad [3]$$

where I_x and I_z are components of the spin vector operator. As the B_1 gradient is to be constant within the sample, we have

$$\alpha(x, \tau_1) = \gamma_n G_1 x \tau_1, \qquad [4]$$

where $G_1 = (\partial B_1(x))/\partial x$.

In the following two limiting situations of coherence evolution during the τ interval are considered. First we treat the case in which coherences are not spoiled during free evolution ($T_2^* > \tau$) and in which demagnetizing-field effects can be neglected (case I). The latter condition means that the external magnetic flux density is low enough. The second, opposite approach takes the demagnetizing field into account and anticipates that all coherences have disappeared at the end of the pulse interval due to transverse relaxation and magnetic field inhomogeneities ($T_2^* \ll \tau$) (case II).

2.1. Case I

In the pulse interval, τ, the coherences represented by Eq. [3] (first term on the right-hand side) evolve in the presence of the main magnetic field gradient G_0 and under the influence of relaxation effects. The latter can be accounted for a posteriori in a phenomenological way as suggested in Ref. (*21*) on the basis of the well-known solutions of the conventional Bloch equations. Both influences are independent of each other and can be treated one after another. The reduced density operator just before the second pulse is then (see Ref. (*13*))

$$\begin{aligned}\sigma(x, \tau_1 + \tau) = {} & I_z[(1 - e^{-(\tau/T_1)}) + \cos\alpha(x, \tau_1)e^{-(\tau/T_1)}] \\ & + [I_y \cos\varphi(x, \tau) + I_x \sin\varphi(x, \tau)] \\ & \times \sin\alpha(x, \tau_1)e^{-(\tau/T_2)}, \end{aligned} \qquad [5]$$

where

$$\varphi(x, t) = \gamma G_0 x t \qquad [6]$$

represents the local phase shift arising from evolution in the gradient of the main magnetic field in a time t. T_1 and T_2 are the longitudinal and transverse relaxation times, respectively.

The second RF pulse, $[\alpha(x, \tau_1)]_x$, converts the density operator into

$$\begin{aligned}&\sigma(x, 2\tau_1 + \tau) \\ &\quad = I_x \sin\varphi(x, \tau)\sin\alpha(x, \tau_1)e^{-(\tau/T_2)} + I_y \\ &\qquad \times \left[\sin\alpha(x, \tau_1)(1 - e^{-(\tau/T_1)}) + \frac{1}{2}\sin 2\alpha(x, \tau_1)e^{-(\tau/T_1)}\right. \\ &\qquad\quad \left. + \frac{1}{2}\sin 2\alpha(x, \tau_1)\cos\varphi(x, \tau)e^{-(\tau/T_2)}\right] \\ &\qquad + I_z[\cos\alpha(x, \tau_1)(1 - e^{-(\tau/T_1)}) + \cos^2\alpha(x, \tau_1)e^{-(\tau/T_1)} \\ &\qquad\quad - \sin^2\alpha(x, \tau_1)\cos\varphi(x, \tau)e^{-(\tau/T_2)}]. \end{aligned} \qquad [7]$$

The I_z term in Eq. [7] represents longitudinal magnetization and does not contribute to the signal. Moreover, demagnetizing fields (see the following section) are negligible at this stage, so that this term can be discarded.

The evolution of spin coherences after the second pulse under the influence of the external field gradient, G_0, and relaxation effects leads to

$$\begin{aligned}&\sigma(x, 2\tau_1 + \tau + t_2) \\ &\quad = [I_x \cos\varphi(x, t_2) - I_y \sin\varphi(x, t_2)] \\ &\qquad \times \sin\alpha(x, \tau_1)\sin\varphi(x, \tau)e^{-(t_2/T_2)}e^{-(\tau/T_2)} \\ &\qquad + [I_x \sin\varphi(x, t_2) + I_y \cos\varphi(x, t_2)] \\ &\qquad \times \left[\sin\alpha(x, \tau_1)(1 - e^{-(\tau/T_1)}) + \frac{1}{2}\sin 2\alpha(x, \tau_1)e^{-(\tau/T_1)}\right. \\ &\qquad\quad \left. + \frac{1}{2}\sin 2\alpha(x, \tau_1)\cos\varphi(x, \tau)e^{-(\tau/T_2)}\right]e^{-(t_2/T_2)}. \end{aligned} \qquad [8]$$

The complex transverse magnetization corresponding to this reduced density operator reads (*20*)

$$\begin{aligned}M_+(x, t) &= M_x(x, t) + iM_y(x, t) \\ &= 2M_0 \mathrm{Tr}\{\sigma(x, 2\tau_1 + \tau + t_2)(I_x + iI_y)\}. \end{aligned} \qquad [9]$$

Carrying out the trace in Eq. [9] results in

$$M_+(x, t) = iM_0 e^{-i\varphi(x, t_2)}\Big[\sin\alpha(x, \tau_1)(1 - e^{-(\tau/T_1)}) \times e^{-(t_2/T_2)} + \frac{1}{2}\sin 2\alpha(x, \tau_1)e^{-(\tau/T_1)}e^{-(t_2/T_2)} - i\sin\alpha(x, \tau_1)\sin\varphi(x, \tau)e^{-((\tau+t_2)/T_2)} - \frac{i}{2}\sin 2\alpha(x, \tau_1)\cos\varphi(x, \tau)e^{-((\tau+t_2)/T_2)}\Big]. \quad [10]$$

The signals to be expected are proportional to the transverse magnetization averaged over all positions x within the sample. This average will be zero unless the terms in Eq. [10] are independent of position.

For the first term in Eq. [10] this condition is met for $t = t_1 + \tau_2 = t_1 + (G_1/G_0)\tau_1$, that is, an echo is expected with the amplitude

$$A(\tau_2) = \frac{M_0}{2}(1 - e^{-(\tau/T_1)})e^{-(\tau_2/T_2)}. \quad [11]$$

The origin of this echo is the unmodulated z-component in Eq. [5] originating from longitudinal relaxation during the evolution interval.

The average of the second term on the right-hand side of Eq. [10] vanishes unless $t = t_1 + 2\tau_2 = t_1 + 2(G_1/G_0)\tau_1$. Correspondingly, an echo appears with the amplitude

$$A(2\tau_2) = \frac{M_0}{4}e^{-(\tau/T_1)}e^{-(2\tau_2/T_2)}. \quad [12]$$

This echo can be traced back to the modulated z-component term in Eq. [5]. Note that this signal will be sensitive to diffusion effects during the τ interval.

The third term in Eq. [10] leads to echoes with maxima at $t = t_1 + \tau \mp \tau_2 = t_1 + \tau \mp (G_1/G_0)\tau_1$. The amplitudes are

$$A(\tau \mp \tau_2) = \pm\frac{M_0}{4}e^{-((2\tau\mp\tau_2)/T_2)}. \quad [13]$$

Finally, the fourth term causes echoes at $t = t_1 + \tau \mp 2\tau_2 = t_1 + \tau \mp 2(G_1/G_0)\tau_1$ with the amplitudes

$$A(\tau \mp 2\tau_2) = \pm i\frac{M_0}{8}e^{-((2\tau\mp 2\tau_2)/T_2)}. \quad [14]$$

These echoes are due to the uncanceled transverse component in Eq. [5]. For the generation of the latter two types of echoes, a gradient G_0 during the evolution interval τ is required, whereas the first two echoes, Eqs. [11] and [12], appear even if the gradient G_0 is applied only after the second pulse.

2.2. Case II

Let us now turn to the limit $T_2^* \ll \tau$, that is, the transverse components at the end of the τ interval are completely spoiled and cannot be refocused. Therefore they need not be considered any longer. The only spin operator term relevant for the formation of echoes is identical with the first term in Eq. [5] and is converted by the second RF pulse into

$$\sigma(2\tau_1 + \tau) = I_z[\cos\alpha(x, \tau_1)(1 - e^{-(\tau/T_1)}) + \cos^2\alpha(x, \tau_1)e^{-(\tau/T_1)}] + I_y\Big[\sin\alpha(x, \tau_1) \times (1 - e^{-(\tau/T_1)}) + \frac{1}{2}\sin 2\alpha(x, \tau_1)e^{-(\tau/T_1)}\Big]. \quad [15]$$

Both terms are modulated along the x-direction. The transverse component evolves from now on in the presence of the demagnetizing field created by the longitudinal component.

The longitudinal component itself is not changed by free evolution and does not contribute to the signal. The corresponding operator term can therefore be dropped. The effect of the demagnetizing field originating from it must, however, be taken into account. The demagnetizing field can be obtained from Eq. [1] as

$$B_d = \mu_0\Delta M_0\cos\alpha(x, \tau_1)(1 - e^{-(\tau/T_1)}) + \mu_0\Delta\frac{M_0}{2}\cos 2\alpha(x, \tau_1)e^{-(\tau/T_1)}, \quad [16]$$

with $\Delta = \frac{1}{2}$ in this case. It originates from the two contributions to the longitudinal magnetization, the modulated one and the unmodulated one. In the above equation we have used $\cos^2\alpha = (\cos 2\alpha + 1)/2$, and we have neglected the contribution to the demagnetizing field coming from the unmodulated part. This unmodulated contribution merely affects the precession frequency and is not responsible for the generation of multiple echoes.

As shown above, multiple echoes are predicted in intervals $\tau_2 = (G_1/G_0)\tau_1$. For a suitable ratio G_1/G_0 these intervals can be adjusted to be short enough to justify the neglect of longitudinal relaxation in these intervals for simplicity. That is, $\tau_2 \ll T_1$. The transverse component evolves under the influence of an external gradient, G_0, and the demagnetizing field given in Eq. [16] according to

$$\sigma(x, 2\tau_1 + \tau + t_2) = [I_y\cos(\varphi(x, t_2) + \varphi_{d1}(x, t_2) + \varphi_{d2}(x, t_2)) + I_x\sin(\varphi(x, t_2) + \varphi_{d1}(x, t_2) + \varphi_{d2}(x, t_2))]$$

$$\times\left[\sin\alpha(x,\tau_1)(1-e^{-(\tau/T_1)})+\frac{1}{2}\sin 2\alpha(x,\tau_1)e^{-(\tau/T_1)}\right]\times e^{-(t_2/T_2)}. \quad [17]$$

The local phase shifts due to the two contributions to the demagnetizing field (see Eq. [16]) are

$$\varphi_{d1}(x,t_2)=\gamma\mu_0\Delta M_0 t_2(1-e^{-(\tau/T_1)})\cos\alpha(x,\tau_1)=\xi_1(t_2)\cos\alpha(x,\tau_1) \quad [18]$$

$$\varphi_{d2}(x,t_2)=\gamma\mu_0\Delta\frac{M_0}{2}t_2e^{-(\tau/T_1)}\cos 2\alpha(x,\tau_1)=\xi_2(t_2)\cos 2\alpha(x,\tau_1). \quad [19]$$

$\varphi(x,t_2)$ is given by Eq. [6].

The complex magnetization can now be computed as

$$\begin{aligned}M_+(x,t)=&\frac{M_0}{2}(1-e^{-(\tau/T_1)})e^{-(t_2/T_2)}\\&\times[e^{-i(\varphi(x,t_2)+\varphi_{d1}(x,t_2)+\varphi_{d2}(x,t_2)-\alpha(x,\tau_1))}\\&\quad-e^{-i(\varphi(x,t_2)+\varphi_{d1}(x,t_2)+\varphi_{d2}(x,t_2)+\alpha(x,\tau_1))}]\\&+\frac{M_0}{4}e^{-(\tau/T_1)}e^{-(t_2/T_2)}\\&\times[e^{-i(\varphi(x,t_2)+\varphi_{d1}(x,t_2)+\varphi_{d2}(x,t_2)-2\alpha(x,\tau_1))}\\&\quad-e^{-i(\varphi(x,t_2)+\varphi_{d1}(x,t_2)+\varphi_{d2}(x,t_2)+2\alpha(x,\tau_1))}]. \quad [20]\end{aligned}$$

Because the signal represents an average over all x-positions in the sample, and in order to analyze the appearance of the echoes, Eq. [20] can be rewritten using the Bessel function expansion (*15*, *22*),

$$e^{i\xi\cos\alpha}=\sum_{n=-\infty}^{+\infty}i^nJ_n(\xi)e^{in\alpha}, \quad [21]$$

and the properties of Bessel functions, $J_n(\xi)$, of integer order,

$$J_{n-1}(\xi)-J_{n+1}(\xi)=2\frac{d}{d\xi}J_n(\xi), \quad [22]$$

$$J_{-n}(\xi)=(-1)^nJ_n(\xi). \quad [23]$$

With these transformations, the exponential terms in Eq. [20] can be expressed as

$$e^{-i(\varphi+\varphi_{d1}+\varphi_{d2}\mp\alpha)}=\pm\sum_{k,m=-\infty}^{+\infty}(-i)^{k-m-1}J_{k-2m\mp1}(\xi_1)J_m(\xi_2)e^{i\gamma x(kG_1\tau_1-G_0t_2)} \quad [24]$$

$$e^{-i(\varphi+\varphi_{d1}+\varphi_{d2}\mp2\alpha)}=\pm i\sum_{k,m=-\infty}^{+\infty}(-i)^{k-m-1}J_{k-2m\mp2}(\xi_1)J_m(\xi_2)e^{i\gamma x(kG_1\tau_1-G_0t_2)}. \quad [25]$$

Equation [20] thus takes the more convenient form,

$$\begin{aligned}M_+(x,t)=&M_0\sum_{k,m=-\infty}^{+\infty}(-i)^{k-m-1}\left\{\frac{(k-2m)}{\xi_1(t_2)}J_{k-2m}(\xi_1(t_2))\right.\\&\times J_m(\xi_2(t_2))(1-e^{-(\tau/T_1)})e^{-(t_2/T_2)}\\&+\frac{i}{4}[J_{k-2m-2}(\xi_1(t_2))+J_{k-2m+2}(\xi_1(t_2))]\\&\left.\times J_m(\xi_2(t_2))e^{-(\tau/T_1)}e^{-(t_2/T_2)}\right\}e^{i\gamma x(kG_1\tau_1-G_0t_2)}. \quad [26]\end{aligned}$$

Equation [26] becomes independent of the position if

$$t_2=k\frac{G_1}{G_0}\tau_1, \quad [27]$$

with $k=1, 2, 3, \ldots$, that is, multiple echoes appear. The amplitude can be computed by employing the approximation for Bessel functions (*22*)

$$J_n(\xi)\cong\frac{1}{n!}\left(\frac{\xi}{2}\right)^n, \quad [28]$$

which applies to times complying to the condition $\xi_i(t_2)\ll 1$ $(i=1, 2)$.

Based on Eq. [26], the amplitude of the echo appearing at the time $t_2=\tau_2=(G_1/G_0)\tau_1$ $(k=1)$ after the second pulse becomes

$$A(\tau_2)=\frac{M_0}{2}(1-e^{-(\tau/T_1)})e^{-(\tau_2/T_2)}+(\text{higher order terms}). \quad [29]$$

The echo at $t_2=2\tau_2=2(G_1/G_0)\tau_1$ $(k=2)$ has the amplitude

$$A(2\tau_2) = \frac{M_0}{4} e^{-(\tau/T_1)} e^{-(2\tau_2/T_2)} + \text{(higher order terms)}. \quad [30]$$

Here we have restricted ourselves to *zero order* terms. The *higher order* terms representing contributions to the amplitude of these echoes due to the demagnetizing field have been neglected. These higher order contributions are expected to produce echoes at $t_2 = 3\tau_2$ ($k = 3$) and $t_2 = 4\tau_2$ ($k = 4$). The echo at $t_2 = 3\tau_2$ has the amplitude

$$A(3\tau_2) = -i \frac{3}{8} \gamma\mu_0 M_0^2 \tau_2 (1 - e^{-(\tau/T_1)}) e^{-(\tau/T_1)} e^{-(3\tau_2/T_2)} + \text{(higher order terms)}. \quad [31]$$

This echo represents mixed contributions from both unmodulated and modulated longitudinal terms in Eq. [5]. No zero order terms exist at this time, and only the *first order* terms were retained. The echo appearing at $t_2 = 4\tau_2$ ($k = 4$) has the amplitude

$$A(4\tau_2) = -i \frac{1}{8} \gamma\mu_0 M_0^2 \tau_2 e^{-(2\tau/T_1)} e^{-(4\tau_4/T_2)} + \text{(higher order terms)}, \quad [32]$$

where only the first order terms have been retained again.

Analyzing the above expressions we conclude that a condition for the observation of higher order echoes is an equilibrium magnetization large enough and/or an interval τ_2 long enough. The position of these echoes can be chosen by varying the ratio G_1/G_0.

3. EXPERIMENTAL

The experiments were carried out at 293 K using a Bruker DPX400 NMR spectrometer. The equilibrium magnetization at $B_0 \approx 9.4$ T is high enough to permit the detection of nonlinear echoes (*15, 17–19*). The gradient of the radiofrequency amplitude was produced with a four-turn conic coil tuned to 400 MHz. It was used both as transmitter and as receiver coil. The dimensions are given in Fig. 1.

In order to avoid perceptible diffusion effects, a poly(dimethyl siloxane) (PDMS) sample with a weight average molecular weight of $M_w = 17{,}000$ and relaxation times $T_1 = 1.52$ s, $T_2 = 318$ ms, was chosen at a test substance. The sample tube diameter was 4 mm with a filling height of 3 mm. The sample was placed in the RF coil as shown in Fig. 1.

The pulse sequence is shown in Fig. 2. τ_1 represents the RF gradient pulse duration and τ the interpulse interval. A constant gradient $G_0 \sim 10$ mT/m of the main magnetic field was applied during the whole pulse sequence by intentionally imperfect shimming. The gradient of the RF amplitude was estimated to be $G_1 \sim 320$ mT/m, which justifies the neglect of sample shape effects. The gradient of the main magnetic field, G_0, was adjusted such that the τ_2 intervals were long enough to avoid nutation multiple echo overlap while ensuring detectable signal intensities. Note that the amplitude of the nonlinear echoes is proportional to τ_2 according to Eqs. [31] and [32].

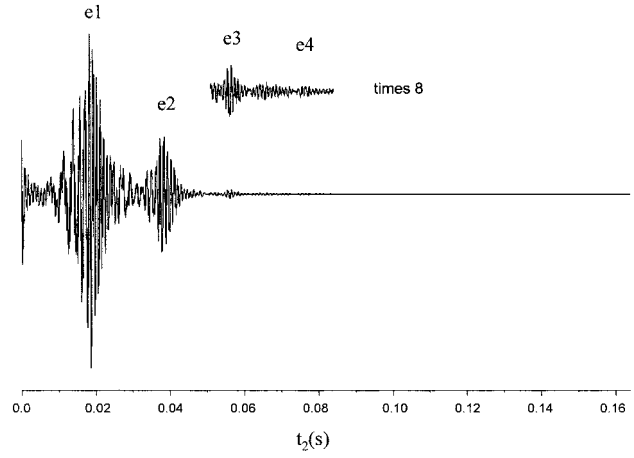

FIG. 3. Echo trains in PDMS 17,000 at 293 K acquired with the aid of the pulse sequence given in Fig. 2 for $\tau_1 = 600$ μs and an interpulse duration $\tau = 750$ ms. A total number of 100 transients was accumulated with a repetition time of 8 s. The echoes appearing at $\tau_2 = 19$ ms ($e1$), $2\tau_2 = 38$ ms ($e2$), $3\tau_2 = 57$ ms ($e3$), and $4\tau_2 = 76$ ms ($e4$) are explained in the text.

Figure 3 shows typical echo trains following the second RF pulse. The pulse width was $\tau_1 = 600$ μs and the pulse spacing $\tau = 750$ ms. In total, 100 transients were accumulated with a repetition time of 10 s. Linear echoes appear at times $t = t_1 + \tau_2 = t_1 + 19$ ms ($e1$) and $t = t_1 + 2\tau_2 = t_1 + 38$ ms ($e2$). Nonlinear echoes (magnified in the figure) are formed at $t = t_1 + 3\tau_2 = t_1 + 57$ ms ($e3$) and $t = t_1 + 4\tau_2 = t_1 + 76$ ms ($e4$) in agreement with the theoretical predictions. Note that, under the present experimental conditions, coherences completely relax during the evolution interval τ.

If the coherences are not completely spoiled during the evolution interval τ, further echo groups appear as shown in Fig. 4 in addition to those shown in Fig. 3. The second group is of a linear character and is predicted in our theoretical description to show up at $t = t_1 + \tau \mp \tau_2$ ($l1$, $r1$) and $t = t_1 + \tau \mp 2\tau_2$ ($l2$, $r2$). The echo amplitudes are given by Eqs. [13] and [14].

In addition, a number of small echoes were observed at $t = t_1 + \tau \mp 3\tau_2$ ($l3$, $r3$) and $t = t_1 + \tau \mp 4\tau_2$ ($l4$, $r4$), respectively. Presumably these are of a nonlinear nature again although they were not considered in the theoretical section above. However, they could be computed numerically with the simulation method suggested in Ref. (*23*).

The echo at $t = t_1 + \tau$ (O) is a conventional Hahn echo produced by the two $\alpha(x)$ pulses provided that the flip angle obeys a relation of the form $\alpha(x) = \alpha_0 + \gamma G_1 x \tau_1$ where, because the amplitude B_1 is not zero at the edge of the coil, $\alpha_0 \neq 0$. This of course is also a matter of how the sample is mounted relative to the RF coil.

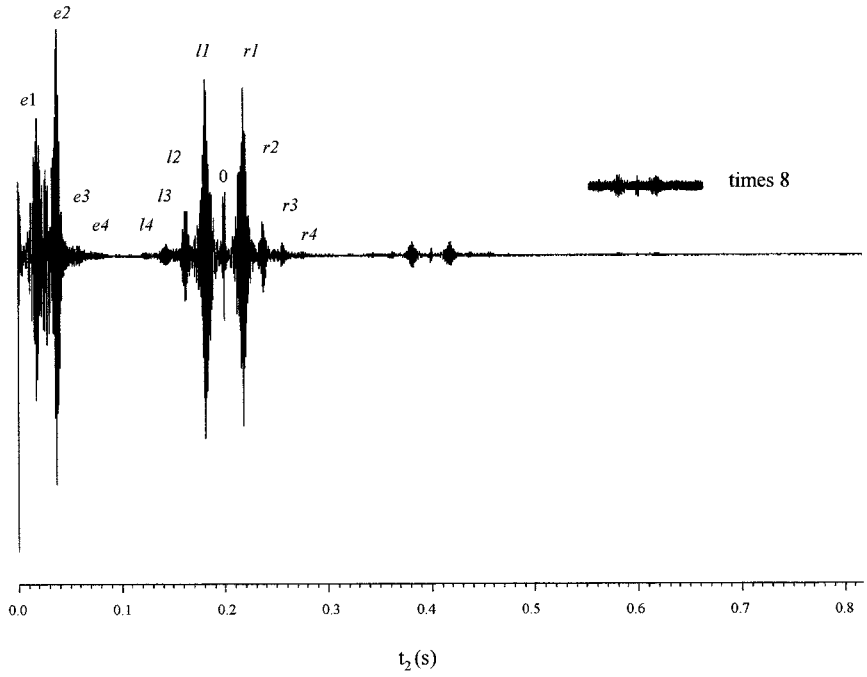

FIG. 4. Echo trains in PDMS 17,000 at 293 K following the pulse sequence shown in Fig. 2 for $\tau_1 = 600$ μs and an interpulse duration $\tau = 200$ μs. A total number of 30 transients was accumulated with a repetition time of 8 s. The first group of echoes $e1 \ldots e4$ is the same as that described in Fig. 2. The second group of echoes (14, ... $r4$) centered at $t = t_1 + \tau = 200$ ms (O) has its origin in the unaveraged transverse component. The third (centered at $t_1 + 2\tau$) and the fourth (centered at $t_1 + 3\tau$) groups represent demagnetizing field effects. The echoes are explained in the text.

The third and the fourth (magnified in the figure) group of echoes represent refocused coherences that can be traced back to the second group. They originate from the evolution of the unaveraged coherences under influence of the demagnetizing field on the same basis as discussed in Refs. (*15, 17*).

Figure 5 represents the intensities of the echoes belonging to the first group as a function of the interpulse interval, $\tau(e1 \ldots e4)$. The curves fitted to the data on the basis of Eqs. [29]–[32] are also indicated (solid line). The fits to the intensity of the first echo using Eq. [29] provides a value for the longitudinal relaxation time, $T_1 = 1.52$ s, in agreement with the value separately measured with the aid of the stimulated echo pulse sequence.

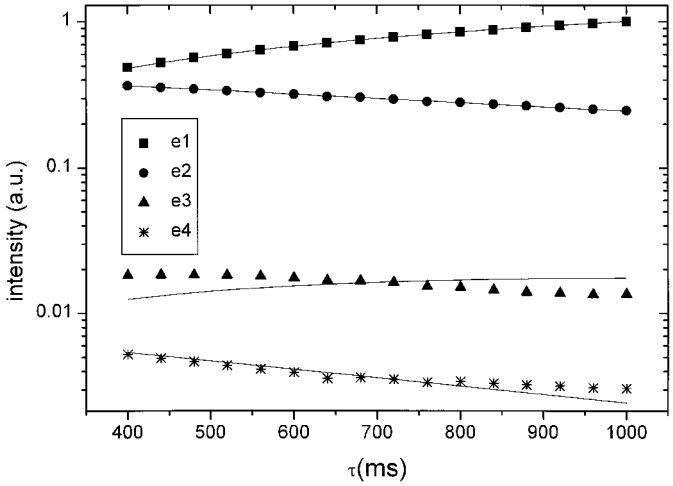

FIG. 5. Intensity of the nutation echoes in PDMS 17,000 at 293 K appearing at $t = t_1 + \tau_2$ ($e1$), $t = t_1 + 2\tau_2$ ($e2$), $t = t_1 + 3\tau_2$ ($e3$), and $t = t_1 + 4\tau_2$ ($e4$) as a function of the evolution interval τ. The solid lines were fitted to the data with the aid of Eqs. [29]–[32]. The echo intensities are plotted to scale.

This T_1 value given, the intensities of all other echoes ($e2$, $e3$, $e4$) can be fitted with only one free parameter. The discrepancy between the theory and experimental data for the nonlinear echoes ($e3$, $e4$) can be explained by an overlap effect with the linear echo appearing at $t = t_1 + 2\tau_2$ as can be seen from Fig. 4. The echoes are represented to scale.

The dependence of the intensity of the second group of echoes on the interpulse duration is shown in Fig. 6. The echo decay allows an estimation of the relaxation time of $T_2 = 318$ ms in agreement with the value measured using an ordinary Hahn spin echo pulse sequence.

4. CONCLUSIONS

In the present work we have shown that multiple nutation echoes are generated by a sequence of two B_1 gradient pulses in the presence of a weak B_0 gradient provided that the gradient directions are the same. No homogeneous 90° reading pulse is needed, so that this experiment can readily be carried out with ordinary instruments. The main field gradient in the strength needed can easily be produced by imperfect shimming.

The gradient of the RF amplitude was produced with the aid

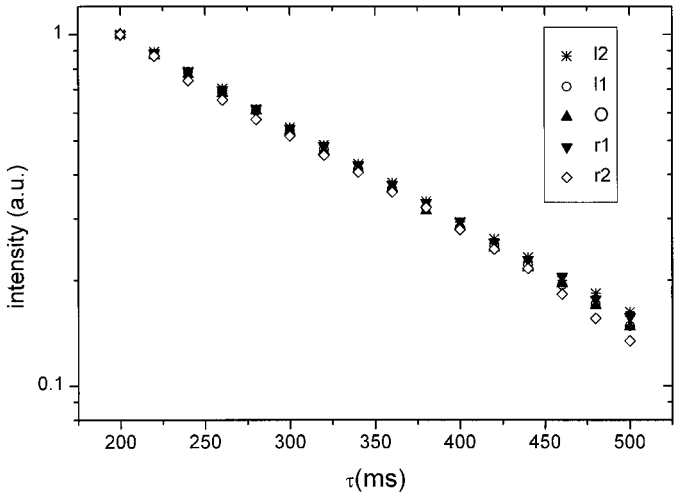

FIG. 6. Normalized intensity of the nutation echoes in Fig. 4 at $t = t_1 + \tau \mp \tau_2$ ($l1$, $r1$), $t = t_1 + \tau \mp 2\tau_2$ ($l2$, $r2$), and $t = t_1 + \tau$ (O) as a function of the evolution interval τ.

of a conic coil which can be used as transmitter and receiver coil. The detection sensitivity of this device turned out to be very favorable. The echo shape obtained with this kind of coil, that is, the linearity of the B_1 distribution, turned out to be superior to that produced by surface coils (*8*), saddle-shape coils (*12*, *14*), or the fringe field of solenoid coils (*5*).

A spin-operator formalism was used for the description of coherence evolution during the pulse sequence in the presence of demagnetizing fields. This formalism has the advantage that it is simple, straightforward, and applicable to *J*-coupled spin systems as well.

The position of the nutation echoes is a function of the gradient ratio G_1/G_0, that is, the echo time is sensitive to the distribution of the RF and main magnetic field gradient in the sample. This suggests applications for localized NMR spectroscopy, for instance. Nutation echoes can also be used for the determination of the self-diffusion coefficient with the advantage that no sophisticated hardware is needed. Furthermore the knowledge of relaxation times is unnecessary. Merely the intensity of the first (at $t = t_1 + \tau_2$) and the second echo (at $t = t_1 + 2\tau_2$) is to be measured as a function of the interpulse interval. The first echo, Eq. [29], is not influenced by diffusion effects because it originates from the unmodulated longitudinal component in Eq. [5]. Therefore, T_1 can be determined on this basis. The second echo (coming from the modulated component) is influenced both by relaxation and by diffusion. Taking the information deduced from the intensities of the two echoes together permits one to determine the diffusion coefficient.

ACKNOWLEDGMENTS

Financial support by the Alexander von Humboldt foundation and the Volkswagen-Stiftung is gratefully acknowledged.

REFERENCES

1. I. Solomon, Rotary spin echoes, *Phys. Rev. Lett.* **2,** 301 (1959).
2. G. S. Karczmar, D. B. Twieg, T. J. Lawry, G. B. Matson, and M. W. Weiner, Detection of motion using B_1 gradients, *Magn. Reson. Med.* **7,** 111 (1988).
3. D. Canet, B. Diter, A. Belmajdoub, J. Brondeau, J. C. Boubel, and K. Elbayed, Self diffusion measurements using a radiofrequency field gradient, *J. Magn. Reson.* **81,** 1 (1989).
4. R. Dupeyre, P. H. Devoulon, D. Bourgeois, and M. Decorps, Diffusion measurements using stimulated rotary echoes, *J. Magn. Reson.* **95,** 589 (1991).
5. R. Kimmich, B. Simon, and H. Köstler, Magnetization-grid rotating-frame imaging technique for diffusion and flow measurements, *J. Magn. Reson. A* **112,** 7 (1995).
6. D. I. Hoult, Rotating frame zeugmatography, *J. Magn. Reson.* **33,** 183 (1979).
7. R. Raulet, D. Grandclaude, F. Humbert, and D. Canet, Fast NMR imaging with B_1 gradients, *J. Magn. Reson.* **124,** 259 (1997).
8. D. Canet, Radio frequency field gradient experiments, *Prog. NMR Spectrosc.* **30,** 101 (1997).
9. M. Garwood and K. Uğurbil, B_1 insensitive adiabatic RF pulses, *NMR Basic Prin. Prog.* **25,** 109 (1992).
10. A. L. Bloom, Nuclear induction in inhomogeneous fields, *Phys. Rev.* **98,** 1105 (1955).
11. R. Kaiser, The edge echo, *J. Magn. Reson.* **42,** 103 (1981).
12. A. Jerschow, Multiple echoes initiated by a single radio frequency pulse in NMR, *Chem. Phys. Lett.* **296,** 466 (1998).
13. R. Kimmich, I. Ardelean, Y. Ya. Lin, S. Ahn, and W. S. Warren, Multiple spin echo generation by gradients of the radio frequency amplitude. Two-dimensional nutation spectroscopy and multiple rotary echoes, *J. Chem. Phys.* **111,** 6051 (1999).
14. J. P. Boehmer, R. I. Prince, and R. W. Briggs, The cone coil, an RF gradient coil for spatial encoding along the B_0 axis in rotating frame imaging experiments, *J. Magn. Reson.* **83,** 152 (1989).
15. G. Deville, M. Bernier, and J. M. Delrieux, NMR multiple echoes observed in solid ^{3}He, *Phys. Rev. B* **19,** 5666 (1979).
16. M. H. Levitt, Demagnetizing field effects in two-dimensional solution NMR, *Concepts Magn. Reson.* **8,** 77 (1996).
17. R. Bowtell, R. M. Bowley, and P. Glover, Multiple echoes in liquids in a high magnetic field, *J. Magn. Reson.* **88,** 643 (1990).
18. I. Ardelean, S. Stapf, D. E. Demco, and R. Kimmich, The nonlinear stimulated echo, *J. Magn. Reson.* **124,** 506 (1997).
19. I. Ardelean, R. Kimmich, S. Stapf, and D. E. Demco, Multiple nonlinear stimulated echoes, *J. Magn. Reson.* **127,** 217 (1997).
20. R. Kimmich, "NMR Tomography, Diffusometry, Relaxometry," Springer-Verlag, Berlin (1997).
21. D. E. Demco, A. Johansson, and J. Tegenfeldt, Constant-relaxation methods for diffusion measurements in the fringe field of superconducting magnets, *J. Magn. Reson. A* **110,** 183 (1994).
22. P. M. Morse and H. Feshbach, "Methods of Theoretical Physics," McGraw–Hill, New York (1953).
23. T. Enss, S. Ahn, and W. S. Warren, Visualizing the dipolar field in solution NMR and MR imaging: three-dimensional structure simulations, *Chem. Phys. Lett.* **305,** 101 (1999).